Hydrogen bonding in cubic $(H_2O)_8$ and $OH\cdot(H_2O)_7$ clusters

Stephen D. Belair and Joseph S. Francisco*
Department of Chemistry and Department of Earth and Atmospheric Science, Purdue University, West Lafayette, Indiana 47906-1393, USA

Sherwin J. Singer†
Department of Chemistry, Ohio State University, Columbus, Ohio 43210, USA
(Received 9 September 2004; published 19 January 2005)

A systematic study is presented for $OH\cdot(H_2O)_7$ clusters derived from the cubic $(H_2O)_8$ octamer by replacing one water with a hydroxyl radical. The system is a prototype for atmospheric water clusters containing the environmentally important OH species, and for OH adsorbed at the surface of ice. The full set of 39 symmetry-distinct cubic $OH\cdot(H_2O)_7$ clusters is enumerated, and the structures are determined using *ab initio* quantum chemical methods. Graph invariants are employed to obtain a unified analysis of the stability and structure of cubic $(H_2O)_8$ and $OH\cdot(H_2O)_7$, relating these physical properties to the various hydrogen-bond topologies present in these clusters. To accomplish this the graph invariant formalism is extended to treat a hydrogen bonding impurity within a pure water network.

DOI: 10.1103/PhysRevA.71.013204 PACS number(s): 36.40.Mr, 02.10.Ox, 36.40.Cg, 31.25.Qm

I. INTRODUCTION

Understanding how gas-phase reactive species in earth's atmosphere become incorporated into cloud droplets or aerosols is essential to determining the complete chemical budgets of these species. Unfortunately, how chemical budgets of reactive species such as gas-phase radicals are impacted by clouds or aerosols is not well understood. Nor has it been systematically addressed. The hydroxyl radical (OH) is a major species in the HO_x chemical family. In fact it is the most important species responsible for the oxidation of pollutants in the atmosphere. A number of field studies are currently addressing the question of what is the abundance of OH in the atmosphere [1–3]. These studies have focus on the gas-phase OH concentrations in the atmosphere. To address the question of the heterogeneous uptake of OH radicals by clouds or aerosols requires that it is understood how OH interacts with water. In 1991, Schaefer and co-workers [4] assumed that the hydroxyl water complex was a $HO\cdots HOH$ structure. Balint-Kurti and co-workers [5] showed that the most stable geometry was $OH\cdots OH_2$. A later study by Xie and Schaefer [6] proposed that the $OH\cdots OH_2$ is the strongly bound OH/water complex. It is only recently that the OH-water complex has been experimentally identified in the laboratory from matrix isolation infrared spectroscopic studies [7,8]. Recent theoretical studies have examined how OH radicals interact with multiple waters up to 6 water molecules [9–11]. These studies address the question of how OH radicals are energetically stabilized by multiple waters. However, the key question that addresses how an OH radical interacts heterogeneously with water is understanding how the hydrogen bonding of OH incorporates itself within the hydrogen bonding topology of water in cloud droplets, aerosols and ice. This question, which is fundamental to understanding how OH fits into the water network, has not been addressed. In order to approach these questions systematically, in this study OH is examined into the hydrogen bonding network of cubic water octamer. The choice of water octamer is motivated by the fact that the water octamer is known to be well ordered [12]. There are 14 unique symmetry structures of the cubic water octamer, each with their own specific hydrogen-bonding topology [13,14].

The $OH\cdot(H_2O)_7$ cluster with oxygen atoms in a roughly cubic arrangement can be constructed in multiple ways (enumerated below) such that all water oxygen atoms are 3-coordinate and the hydroxyl radical is involved in two H-bonds. This type of hydrogen-bond isomerism, fixed oxygens connected by a variable H-bond arrangement constrained by the ability of the water molecule to donate to at most two H-bonds and accept at most two H-bonds, occurs in many aqueous systems. It is responsible for the zero-point entropy of ice-Ih [15,16], and is also found in ice-VII and ice-III [17,18]. As mentioned above, the cubic water octamer can form 14 isomers [13,14], of which the most stable D_{2d} and S_4 isomers have been observed experimentally [12]. It has long been recognized that the topological arrangement of H-bonds can be summarized by oriented graphs [19–26]. It has also been noted that physical properties, such as the energy, of H-bond isomers can be linked to the topology of the H-bonds [13,21–23,27,28]. In these works, the topological features of the H-bond network that were correlated with physical properties were identified in an *ad hoc* fashion.

Recently, we introduced a systematic way of identifying topological features of an H-bond network in water clusters [24] and periodic ice crystals [25]. Scalar physical properties must depend features that are invariant to symmetry operation of the system. Hence, the appropriate features of the H-bond topology, which we call *graph invariants*, are linear combinations of variables describing the H-bond topology that are unchanged by all symmetry operations. The graph invariants can be arranged in a hierarchy of increasing complexity, providing a sequence of approximation that can be generated until suitable convergence is attained. To date, we

*Email address: francisc@purdue.edu
†Email address: singer@chemistry.ohio-state.edu

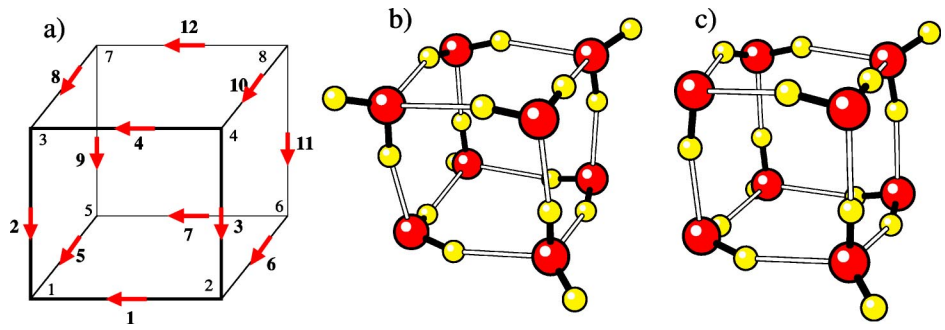

FIG. 1. (a) Canonical bond directions adopted for description of the cubic $(H_2O)_8$ and $OH\cdot(H_2O)_7$ clusters. The vertex labels are in regular type and the bond labels are in bold face next to the arrows. (b) $(H_2O)_8$ isomer of D_{2d} symmetry. (c) $OH\cdot(H_2O)_7$ cluster, designated as D_{2d}^{OH} in the text, obtained by removing a dangling hydrogen from the left, upper front water of the center $(H_2O)_8$ cluster.

have only applied graph invariants to either pure water clusters $(H_2O)_n$ or pure ice. All other topological analyses of water clusters have been limited to $(H_2O)_n$ [21–23,27,28]. This work provides the first topological analysis of hydrogen bonding near an impurity.

In this work we present a formalism for treating a mixture of more than one hydrogen bonding species with graph invariants. Besides the analysis of solutes in water clusters, current interest in impurities embedded in ice [18,29–33] furnishes another motivation for developing these theoretical methods. On the experimental side, self-trapping by reorientation of the H-bonds, involving the type of H-bond isomerism we study in this work, has been invoked to explain the absence of observed diffusion of H_3O^+ in low temperature ice [34]. Theoretical treatments of point defects in ice at the molecular level are beginning to appear [30–33]. It has been emphasized that distant shells (e.g., up to the 18th shell [33]) surrounding a charged defect in ice must be included to converge properties like the solvation energy. To date, the H-bond topology has not been carefully considered in the treatments of point defect in ice. Given the large number of H-bond arrangements and large energy barriers separating them, direct simulation of the possible H-bond arrangements surrounding defects in ice would be difficult, pointing to the need for analytical methods to extend the reach of simulations. The present work is an essential step in that direction.

The concept and use of graph invariants is explained in Sec. II. We then demonstrate how graph invariants link energy, dipole moment, and other physical properties with the hydrogen bond topology of the H-bond isomers of cubic $(H_2O)_8$, treated in Sec. III, and $OH\cdot(H_2O)_7$, treated in Sec. IV.

II. GRAPH INVARIANTS

With the exception of high pressure phases of ice, the hydrogen atom is not shared equally between hydrogen bound water molecules. Hydrogen bonds are therefore directional, with the direction usually taken to point from hydrogen donor to hydrogen acceptor. As detailed in Secs. III and IV, many isomers of $(H_2O)_8$ and $OH\cdot(H_2O)_7$ exist which have similar oxygen atom geometries but differ in the direction of the hydrogen bonds. In ordered aqueous systems, physical properties are sometimes captured by a reduced description in terms of the H-bond topology of the structure—specifying which waters are connected by H-bonds and the directionality of those bonds [13,21,24]. Physical properties beyond the topology, like bond lengths, bond angles, energies, an dipole moments, can then be linked to the H-bond topology.

To track the H-bond topology, we introduce bond variables b for each hydrogen bond which takes the values +1 or −1 depending on the direction of H-bond in a particular structure relative to an arbitrarily chosen canonical direction. The canonical directions of H-bonds we chose for $(H_2O)_8$ and $OH\cdot(H_2O)_7$ cubes are shown in Fig. 1(a).

In Fig. 1(b), the physical $(H_2O)_8$ cluster of D_{2d} symmetry is shown. Comparing the canonical bond direction given in Fig. 1(a) with the physical cluster of Fig. 1(b), the H-bond topology of the D_{2d} structure is specified by $b_1=-1$, $b_2=+1$, $b_3=-1$, $b_4=+1$, $b_5=-1$, $b_6=+1$, $b_7=+1$, $b_8=+1$, $b_9=-1$, $b_{10}=-1$, $b_{11}=+1$, and $b_{12}=-1$.

Consider optimizing the geometry of a $D_{2d}(H_2O)_8$ structure specified by bond variables b_r, $r=1,\ldots12$ given above. Then consider optimizing a second initial structure, also having D_{2d} symmetry but with bond variables generated from those specified above by one of the rotations or reflection operations of the cube. Clearly, the scalar physical properties—energy, magnitude of dipole moment, bond lengths—of the original structure, and the rotated or reflected structure would be identical. Hence, if these properties are linked to H-bond topology, they must depend on the b_r's in combinations that are invariant to symmetry operations of the cube. These combinations, which we call *graph invariants*, are obtained by application of a group theoretical projection operator on any bond variable b_r,

$$I_r(b_1,\ldots,b_{12}) = \frac{1}{48}\sum_{\alpha=1}^{48} g_\alpha(b_r), \tag{1}$$

on any product of two bond variables b_rb_s,

$$I_{rs}(b_1,\ldots,b_{12}) = \frac{1}{48}\sum_{\alpha=1}^{48} g_\alpha(b_rb_s), \tag{2}$$

three bond variables $b_rb_sb_t$, and so on. We call projections on single bond variables like I_r first-order invariants, projections

on products of two bond variables like I_{rs} second order invariants, and so on. Since we expect some localization of the topological properties that determine physical properties, we expect the low order invariants to be more important than high order ones, and to date this has been borne out in all cases studied.

If H-bond topology predicts a scalar physical property, then that property must depend upon the topology, i.e., the bond variables, in symmetry-invariant combinations like Eqs. (1) and (2). For example, the energy must be a function of first-order invariants, second order invariants, third order invariants, and so on,

$$E(b_1,b_2,\ldots)=\mathcal{E}\Big[\underbrace{I_r(b_1,b_2,\ldots),I_s(b_1,b_2,\ldots),\ldots}_{\text{first-order invariants}},\underbrace{I_{rs}(b_1,b_2,\ldots),I_{tu}(b_1,b_2,\ldots),\ldots}_{\text{second-order invariants}},\ldots\Big]. \tag{3}$$

In principle, the function $\mathcal{E}$ may take any form. In practice, we have found that the simplest linear expansion is adequate:

$$E(b_1,b_2,\ldots)=\underbrace{\sum_r \alpha_r I_r(b_1,b_2,\ldots)}_{\text{first-order}}+\underbrace{\sum_{rs} \alpha_{rs} I_{rs}(b_1,b_2,\ldots)}_{\text{second-order}}+\underbrace{\sum_{rst} \alpha_{rst} I_{rst}(b_1,b_2,\ldots)}_{\text{third-order}}+\cdots. \tag{4}$$

The effectiveness of a linear expansion in the lowest order, leading invariants is confirmed in this work. Below, energy and other physical properties are calculated by semiempirical and *ab initio* quantum chemical methods for a large number of H-bond isomers. This information constitutes the left-hand side of Eq. (4). The right hand side of Eq. (4), containing far fewer α-coefficients than data points for the left-hand side, is determined by least squares fit. In this way, *ab initio* data can be interpolated, as we have done for the many isomers of the $(H_2O)_{20}$ dodecahedron [24], or extrapolated, as we have done to predict proton-ordering phase transitions in ice from *ab initio* calculations for small unit cells [35]. Adding higher order invariants to the right side of Eq. (4) will make the least squares fit more accurate at the expense of greater complexity and the ability to predict many properties from as little data as possible. Eventually, when a complete set of invariants is added to the right side of Eq. (4) the expansion is useless as an interpolation or extrapolation tool because the number of α-parameters equals the number of symmetry-distinct H-bond isomers.

There are no first order graph invariants for the $(H_2O)_8$ cube. In other words, application of the projection operator on any bond variable as in Eq. (1) gives zero. The second order invariants [Eq. (2)] furnish the leading order description of physical properties in terms of graph invariants. There are five such second order invariants, given below:

$$I_{4,7}=\frac{1}{6}(b_4b_7+b_6b_8+b_3b_9+b_5b_{10}+b_2b_{11}+b_1b_{12}), \tag{5}$$

$$\begin{aligned} I_{1,9}=\frac{1}{24}(&-b_3b_5-b_4b_5-b_2b_6+b_4b_6-b_2b_7+b_3b_7-b_1b_8\\ &+b_3b_8+b_7b_8-b_1b_9+b_4b_9+b_6b_9+b_1b_{10}+b_2b_{10}\\ &-b_7b_{10}-b_9b_{10}+b_1b_{11}-b_4b_{11}+b_5b_{11}-b_8b_{11}+b_2b_{12}\\ &-b_3b_{12}+b_5b_{12}-b_6b_{12}), \end{aligned} \tag{6}$$

$$\begin{aligned} I_{2,3}=\frac{1}{12}(&b_2b_3+b_1b_4+b_5b_6+b_1b_7+b_5b_8+b_2b_9+b_6b_{10}\\ &+b_8b_{10}+b_3b_{11}+b_9b_{11}+b_4b_{12}+b_7b_{12}), \end{aligned} \tag{7}$$

$$\begin{aligned} I_{1,3}=\frac{1}{24}(&-b_1b_2+b_1b_3+b_2b_4-b_3b_4-b_1b_5-b_2b_5+b_1b_6\\ &-b_3b_6+b_5b_7-b_6b_7+b_2b_8-b_4b_8+b_5b_9-b_7b_9-b_8b_9\\ &+b_3b_{10}+b_4b_{10}+b_6b_{11}+b_7b_{11}-b_{10}b_{11}+b_8b_{12}+b_9b_{12}\\ &-b_{10}b_{12}-b_{11}b_{12}), \end{aligned} \tag{8}$$

$$\begin{aligned} I_{1,1}=\frac{1}{12}(&b_1^2+b_2^2+b_3^2+b_4^2+b_5^2+b_6^2+b_7^2+b_8^2+b_9^2+b_{10}^2+b_{11}^2\\ &+b_{12}^2). \end{aligned} \tag{9}$$

We have labeled the invariants by the indices of a bond pair which generates the invariant by application of a projection operator as in Eqs. (1) and (2). Since several different sets of bond variables can generate the same invariant, there could be many choices for how to label the invariants, although the actual invariant are indeed unique.

So far we have only discussed the pure water $(H_2O)_8$ cubes. When an OH radical is substituted for a water molecule, the bond still has directionality but is chemically distinct. In an oriented graph, we may introduce bonds of a different color to indicate H-bonds containing an H-bonding impurity like the OH radical. When constructing graph invariants, we introduce new bond variables to indicate each chemically distinct H-bond. For the $OH\cdot(H_2O)_7$ cluster, a second type of bond variable c_r is used to represent the different colored bonds. We use $c_r=0$ to indicate the absence of an OH radical, and $c_r=\pm 1$ to indicate the direction of the OH when the radical is present. Similarly, the absence of a water at the rth H-bond is indicated by setting $b_r=0$. Hence, the cubic pure water clusters are specified by 12 water bond

variables $b_r = \pm 1$, and all OH bond variables $c_r = 0$, while the $OH \cdot (H_2O)_7$ cubes are described by setting one of the b_r variables equals zero and the c_r variable at the same bond equal to ± 1.

In Fig. 1(c) we show the physical $OH \cdot (H_2O)_7$ cube obtained by removing a dangling hydrogen from the upper, left, front water molecule of the $(H_2O)_8$ in the center. In our labeling scheme, to be explained below, this $OH \cdot (H_2O)_7$ cluster is designated as $D_{2d}^{OH(1)}$. The H-bond topology of the $D_{2d}^{OH(1)}$ would be captured by setting $b_1 = -1$, $b_2 = 0$, $b_3 = -1$, $b_4 = +1$, $b_5 = -1$, $b_6 = +1$, $b_7 = +1$, $b_8 = +1$, $b_9 = -1$, $b_{10} = -1$, $b_{11} = +1$, and $b_{12} = -1$, the same as in Fig. 1 except that $b_2 = 0$. Also, to specify the $OH \cdot (H_2O)_7$ configuration of Fig. 1, we set $c_2 = +1$ and $c_j = 0$ for $j = 1, 3, 4, \ldots, 12$. Structures that involve more than one OH radical would be denoted by more than one non-zero c variable, and more than one type of hydrogen-bonding impurity would would call for other types of bond variables. The $(H_2O)_8$ and $OH \cdot (H_2O)_7$ structures studied in this work do not call for those extensions, although the graph theoretical formalism can treat these cases.

The graph invariants for the $OH \cdot (H_2O)_7$ cubes involve one nonzero c variable. The leading order invariants for the $OH \cdot (H_2O)_7$ structures are the second order invariants, Eqs. (1)–(9), which are obtained for $OH \cdot (H_2O)_7$ when the projector operates on a product of two b bond variables, plus a set of second order invariants obtained when the projector operators on the product $b_r c_s$. This gives five more invariants:

$$I_{12,c1} = \frac{1}{12}(b_{12}c_1 + b_{11}c_2 + b_9c_3 + b_7c_4 + b_{10}c_5 + b_8c_6 + b_4c_7 + b_6c_8 + b_3c_9 + b_5c_{10} + b_2c_{11} + b_1c_{12}), \tag{10}$$

$$\begin{aligned} I_{10,c1} = \frac{1}{48}(&- b_8c_1 - b_9c_1 + b_{10}c_1 + b_{11}c_1 - b_6c_2 - b_7c_2 + b_{10}c_2 + b_{12}c_2 - b_5c_3 + b_7c_3 + b_8c_3 - b_{12}c_3 - b_5c_4 + b_6c_4 + b_9c_4 - b_{11}c_4 \\ &- b_3c_5 - b_4c_5 + b_{11}c_5 + b_{12}c_5 - b_2c_6 + b_4c_6 + b_9c_6 - b_{12}c_6 - b_2c_7 + b_3c_7 + b_8c_7 - b_{10}c_7 - b_1c_8 + b_3c_8 + b_7c_8 - b_{11}c_8 - b_1c_9 \\ &+ b_4c_9 + b_6c_9 - b_{10}c_9 + b_1c_{10} + b_2c_{10} - b_7c_{10} - b_9c_{10} + b_1c_{11} - b_4c_{11} + b_5c_{11} - b_8c_{11} + b_2c_{12} - b_3c_{12} + b_5c_{12} - b_6c_{12}), \end{aligned} \tag{11}$$

$$\begin{aligned} I_{4,c1} = \frac{1}{24}(&b_4c_1 + b_7c_1 + b_3c_2 + b_9c_2 + b_2c_3 + b_{11}c_3 + b_1c_4 + b_{12}c_4 + b_6c_5 + b_8c_5 + b_5c_6 + b_{10}c_6 + b_1c_7 + b_{12}c_7 + b_5c_8 + b_{10}c_8 + b_2c_9 \\ &+ b_{11}c_9 + b_6c_{10} + b_8c_{10} + b_3c_{11} + b_9c_{11} + b_4c_{12} + b_7c_{12}), \end{aligned} \tag{12}$$

$$\begin{aligned} I_{3,c1} = \frac{1}{48}(&- b_2c_1 + b_3c_1 - b_5c_1 + b_6c_1 - b_1c_2 + b_4c_2 - b_5c_2 + b_8c_2 + b_1c_3 - b_4c_3 - b_6c_3 + b_{10}c_3 + b_2c_4 - b_3c_4 - b_8c_4 + b_{10}c_4 - b_1c_5 \\ &- b_2c_5 + b_7c_5 + b_9c_5 + b_1c_6 - b_3c_6 - b_7c_6 + b_{11}c_6 + b_5c_7 - b_6c_7 - b_9c_7 + b_{11}c_7 + b_2c_8 - b_4c_8 - b_9c_8 + b_{12}c_8 + b_5c_9 - b_7c_9 \\ &- b_8c_9 + b_{12}c_9 + b_3c_{10} + b_4c_{10} - b_{11}c_{10} - b_{12}c_{10} + b_6c_{11} + b_7c_{11} - b_{10}c_{11} - b_{12}c_{11} + b_8c_{12} + b_9c_{12} - b_{10}c_{12} - b_{11}c_{12}), \end{aligned} \tag{13}$$

$$I_{1,c1} = \frac{1}{12}(b_1c_1 + b_2c_2 + b_3c_3 + b_4c_4 + b_5c_5 + b_6c_6 + b_7c_7 + b_8c_8 + b_9c_9 + b_{10}c_{10} + b_{11}c_{11} + b_{12}c_{12}). \tag{14}$$

Note that the bond variable function in Eqs. (5)–(14) are invariant with respect to the placement of the OH radical (nonzero c-variable) within the cluster. Even though the labels in these equations reflect the fact that they could be generated by projection with a nonzero c-variable at bond 1, the complete invariant is symmetric with respect to the placement of the c bond, as it should be. Some of the invariants given in Eqs. (5)–(14) have rather trivial values. For example, $I_{1,c1}$ will always have the value zero for the physical clusters considered here because a water and OH radical cannot occupy the same H-bond position. However, mathematically it is one of the second order invariants and for completeness is listed here. If nonzero c variables could appear in more than one location, which would corresponding to multiple insertions of hydroxyl into the cluster, then more invariants would need to be considered.

III. $(H_2O)_8$

It has been shown previously that there are 14 symmetry-unique configurations for the cubic water octamer [13]. The stability of the 14 isomers was estimated using the empirical OSS2 potential [36,37], which compared favorably with *ab initio* data available for a subset of the isomers from calculations performed by Tsai and Jordan [38]. In this work, the energy of the clusters was observed to depend most strongly on a particular topological feature, the number of nearest

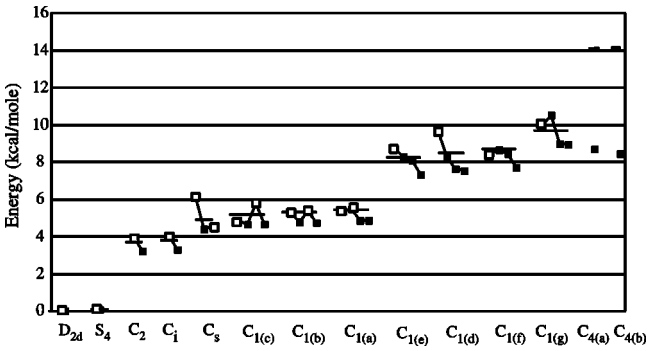

FIG. 2. Relative energies of the H-bond isomers of cubic $(H_2O)_8$ (short horizontal lines) and $OH\cdot(H_2O)_7$ (squares). Unfilled squares represent the energies of $OH\cdot(H_2O)_7$ structures formed by removing the dangling hydrogen of a dimer unit. The solid squares represent the energies of $OH\cdot(H_2O)_7$ structures formed by removing the dangling hydrogen of another site.

neighbor dangling hydrogen pairs in the cluster. In a more recent study [14], in which *ab initio* optimizations were performed on each of the 14 structures, an order of stability was established and it was found that this order could be explained by counting the numbers of occurrences of certain topological features that each conformer exhibited, none of which were identified explicitly as the number of nearest neighbor dangling hydrogen pairs. Neither of these previous studies used graph invariants. In this section, we reanalyze the water cube, and show how graph invariants provide a systematic alternative to what are otherwise *ad hoc* analyses.

The energies of the 14 cubic $(H_2O)_8$ octamers calculated with second order Moeller-Plesset perturbation theory (MP2) [39–43] using a 6-31G* basis set are indicated by the short horizontal lines in Fig. 2. The 14 cubic $(H_2O)_8$ clusters that label the *x* axis of Fig. 2 are designated according to their point group symmetry, and clusters with the same symmetry are differentiated with additional letter (a), (b), …. Drawings of each of the 14 $(H_2O)_8$ isomers can be found in Fig. 3 of Ref. [14]. The 6-31G* basis was chosen because it is a medium quality basis set that can be used with the MP2 correlation method to produce reliable results for large open-shell clusters. The Gaussian98 program was used for all the electronic structure calculations [44]. Tabulated energies and pictures of each structure can be found in on-line supplementary materials [45].

Before presenting an analysis of in terms of invariants, it is useful to summarize how cubic $(H_2O)_8$ was previously analyzed by two research groups. Within any of the conformers of the cubic water octamer, each water molecule is bound in one of two configurations. It can accept a hydrogen at only one of its lone pairs and donates both of its hydrogens for hydrogen bonding, like the water molecule at the top, right front in the $(H_2O)_8$ cluster of Fig. 1(b). Alternatively, a water can accept hydrogens at both of the lone pairs of its oxygen, and donates only one of its own hydrogens for bonding while the other hydrogen is dangling. The water molecule at the top, left front of Fig. 1(b) is an example. These two cases are referred to as double donor and double acceptor, respectively. The number of nearest neighbor dangling hydrogens pairs, tracked by McDonald *et al.* [13], is therefore the number of nearest neighbor double acceptors.

TABLE I. Value of second order invariants for the 14 cubic $(H_2O)_8$ octamers.

Structure	$I_{4,7}$	$I_{1,9}$	$I_{2,3}$	$I_{1,3}$	$I_{1,1}$
D_{2d}	1	$-\frac{1}{3}$	-1	$\frac{1}{3}$	1
S_4	$-\frac{1}{3}$	$\frac{1}{3}$	$-\frac{1}{3}$	$\frac{1}{3}$	1
C_2	$\frac{1}{3}$	$-\frac{1}{3}$	$-\frac{2}{3}$	$\frac{1}{3}$	1
C_i	-1	$\frac{1}{3}$	0	$\frac{1}{3}$	1
C_s	$-\frac{2}{3}$	$\frac{1}{3}$	0	$\frac{1}{3}$	1
$C_{1(c)}$	0	0	$-\frac{1}{3}$	$\frac{1}{3}$	1
$C_{1(b)}$	$\frac{2}{3}$	$-\frac{1}{3}$	$-\frac{2}{3}$	$\frac{1}{3}$	1
$C_{1(a)}$	$-\frac{2}{3}$	$\frac{1}{3}$	0	$\frac{1}{3}$	1
$C_{1(d)}$	$-\frac{1}{3}$	$\frac{1}{6}$	0	$\frac{1}{3}$	1
$C_{1(e)}$	$-\frac{1}{3}$	$\frac{1}{6}$	0	$\frac{1}{3}$	1
$C_{1(f)}$	$\frac{1}{3}$	$-\frac{1}{6}$	$-\frac{1}{3}$	$\frac{1}{3}$	1
$C_{1(g)}$	0	$\frac{1}{6}$	0	$\frac{1}{3}$	1
$C_{4(a)}$	1	$-\frac{1}{3}$	$-\frac{1}{3}$	$\frac{1}{3}$	1
$C_{4(b)}$	$-\frac{1}{3}$	$\frac{1}{3}$	$\frac{1}{3}$	$\frac{1}{3}$	1

The first part of the structural analysis performed by Belair and Francisco [14] was based on the idea that it is possible to orient a pair of water molecules within a cubic water octamer so that they have an orientation very similar to the fully optimized water dimer. This dimer unit within the octamer framework consists of a double acceptor water molecule donating one of its hydrogens to a double donor. In Fig. 1(b), the four vertical H-bonds are in a dimer configuration, while the other eight horizontal H-bonds are not dimers. When one counts the number of these dimers in each structure, it is apparent that the most stable structures have the greatest number of dimers.

McDonald *et al.* [13] found the number of nearest neighbor dangling hydrogens was the most important factor governing the stability of the $(H_2O)_8$ octamer, while Belair and Francisco [14] identified the number of dimers as the crucial structural feature. Actually, these features turn out to be the same topological property for cubic $(H_2O)_8$. As shown in the following analysis using graph invariants, both features are a linear combination of second order invariants and $n_{dimer}=4-n_{n.n.dangling\ H\cdot}$.

The values of the second order invariants are obtained by assigning the bond variables for each of the 14 structures, as we illustrated for the D_{2d} isomer in the discussion of Fig. 1, and then evaluating expressions Eqs. (5)–(9). The result is given in Table I. Each column in this table can be thought of as a basis vector for describing physical properties of the cube in terms of H-bond topology. First, notice that $I_{1,1}$ is 3 times $I_{1,3}$. Even though the invariants area all algebraically independent, linear dependences arise when evaluated for particular structures because of the physical constraints of aqueous hydrogen bonding (e.g., accepting and donating at most two H-bonds for neutral water molecules—what are called the "ice rules" in the solid phase [46]). If, for example, H_3O^+ or OH^- units within the octamer were allowed, some of the linear dependences observed in Table I would be broken. For cubic $(H_2O)_8$, we eliminate one of the linearly de-

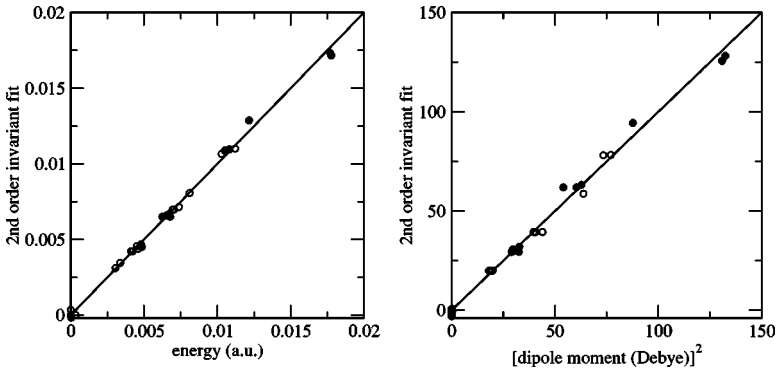

FIG. 3. Comparison of semiempirical PM3 (open circles) and *ab initio* MP2 results (filled circles) with fits to second order invariants for the cubic water octamer. Energy is shown on the left and squared dipole moment on the right. The energy of the most stable octamer is chosen as the zero of energy.

pendent invariants, chosen with no loss of generality to be $I_{1,3}$, to obtain 4 linearly independent vectors. Hence, the second order invariants provide 4 independent parameters for describing scalar physical properties of the 14 octamers, of which $I_{1,1}$ is a constant. In terms of second order invariants,

$$n_{dimer} = 6I_{1,9} - 6I_{2,3}, \quad n_{n.n.dangling\ H} = 4 - 6I_{1,9} + 6I_{2,3}. \tag{15}$$

A description at the level of second order invariants, would have automatically accounted for dimers or nearest neighbor dangling hydrogens, and two other topological features at the level of second order invariants. Incorporating higher order invariants would involve more topological features, although these higher order invariants do not appear to be important for the case at hand.

Having discussed the relationship between graph invariants and previously used topological parameters, we now turn to least squares fitting of physical properties as described in Eq. (4). The plots in Fig. 3 give the results of fitting the energy and squared dipole moment of $(H_2O)_8$ to a linear combination of the leading order graph invariants, the second order invariants. We treated the dipole moment to illustrate that scalar properties besides the energy could be fit with graph invariants. The choice of fitting the squared dipole moment is based on a bond dipole model: If the total dipole moment can be written as a sum of dipoles whose direction is controlled by the bond variables b_r, then the squared dipole moment is a symmetry-invariant that is quadratic in the bond variables, i.e., a second-order invariant. The fit given in Fig. 3 confirms that (1) physical properties of cubic $(H_2O)_8$ can indeed be correlated with the H-bond topology, and (2) that a linear combination of the second order invariants compactly describes the link to H-bond topology.

Energy and squared dipole moment from PM3 [47] and MP2 [39–43] level calculations of the 14 octamers are compared with a linear fit to the 4 linearly independent second order invariants, one of which is an overall constant. It should be noted that Fig. 3 represents the lowest level invariant description, in that we are taking the lowest order nonzero invariants (the second order invariants), and using a linear fit. In other situations, description of physical properties might require higher order invariants or might depend on invariants in a nonlinear fashion. In view of the success of the linear fits in Fig. 3, we did not seek to improve the description beyond the simplest level. The fitting coefficients are given below in Table II in conjunction with a discussion of the transferability of parameters between $(H_2O)_8$ and $OH\cdot(H_2O)_7$.

After establishing the number of dimers (property *D* of their Table I) as an important topological feature, subsequent parts of Belair and Francisco's analysis sought a more accurate relationship between topology and physical properties by considering additional topological features of the water octamer [14]. Unlike parameters generated by invariant theory, these topological features were chosen in an *ad hoc* and more complicated fashion, although we will show that they were nearly as effective as the second order invariants. To describe this portion of Belair and Francisco's analysis, it is necessary to view the cubic water octamer, in each of three directions, as a pair of cyclic water tetramers bound together by 4 hydrogen bonds where each of the four hydrogens are donated by one or the other of the tetramers. That analysis revealed that the least stable cubes have, in exactly one direction, all four of the donated hydrogens coming from one of the tetramers, and that the most stable cubes have, in all three directions, two hydrogens donated by each tetramer, and that the remaining cubes have, in 1, 2, or 3 directions, 3 hydrogens donated by one tetramer and 1 by the other. This number is listed as property *A* in Table I of Ref. [14].

The order was further resolved by counting, when *A* took the value of either 2 or 4, the number of directions in which the pairs of donated hydrogens coming from a particular tetramer were on adjacent (across an edge) or diagonal (across a face) water molecules. It was found that the more stable structures exhibited more occurrences of the diagonal configuration. This is property *B* of Table I of Ref. [14]. When *A* took a value of 3, the group of octamers with intermediate stability, the number of directions in which three of the hydrogens were donated by one tetramer was reported as property *B* in Table I of Ref. [14]. From this, it was found that, of this middle group, the most stable structures had this property in only 1 direction while the least stable structure had this property in all 3 directions.

Although Belair and Francisco did not attempt a linear fit, Fig. 4 shows that a fit with 4 parameters, the topological properties *D*, *A*, *B* described in their work plus a constant, does yield a reasonably good description of the dependence of energy on H-bond topology. Property *D* (dimers) is a second order invariant, while properties *A* and *B* are not second order invariants and must be higher order invariants. Comparing with Fig. 3, the accuracy is close to second order

TABLE II. Coefficients obtained by fitting energy and squared dipole moment of cubic $(H_2O)_8$ and $OH\cdot(H_2O)_7$ isomers to a linear combination of graph invariants. Invariants $I_{4,7}$, $I_{1,9}$ and $I_{2,3}$ are used in the fit of both $(H_2O)_8$ and $OH\cdot(H_2O)_7$ isomers. Comparison is made between the fitting coefficients for these three invariants when just the 14 $(H_2O)_8$ isomers are fit, versus fitting across the entire set of $(H_2O)_8$ and $OH\cdot(H_2O)_7$ isomers. The last five invariants are only used in the fit of $OH\cdot(H_2O)_7$ properties. Invariant $I_{1,3}$ is a constant for all the $(H_2O)_8$ isomers, but does change value for the $OH\cdot(H_2O)_7$ topologies. Therefore, even though $I_{1,3}$ only involves H bonds of water molecules, it only appears in the simultaneous fit of $(H_2O)_8$ and $OH\cdot(H_2O)_7$ properties. When properties of $OH\cdot(H_2O)_7$ calculated at the MP2 level are fit, the two isomers shown in Fig. 6 are not included because their H-bond topology differs from the rest of the clusters.

	Energy (a.u.)		Squared dipole moment (D^2)	
Invariant parameter	PM3	MP2	PM3	MP2
$I_{4,7}$ [$(H_2O)_8$ only]	0.00332	0.00599	57.7	97.4
$I_{4,7}$ [$(H_2O)_8$ and $OH\cdot(H_2O)_7$]	0.00314	0.00671	51.3	87.7
$I_{1,9}$ [$(H_2O)_8$ only]	−0.00986	−0.0143	−1.64	−0.230
$I_{1,9}$ [$(H_2O)_8$ and $OH\cdot(H_2O)_7$]	−0.00993	−0.0150	−9.61	−18.9
$I_{2,3}$ [$(H_2O)_8$ only]	0.0160	0.0260	117	191
$I_{2,3}$ [$(H_2O)_8$ and $OH\cdot(H_2O)_7$]	0.0157	0.0283	113	191
$(H_2O)_8$ and $OH\cdot(H_2O)_7$				
$I_{1,3}$	0.0205	−0.00710	155	227
$I_{12,c1}$	0.00437	0.0105	131	212
$I_{10,c1}$	−0.0225	−0.0208	−35.1	−76.4
$I_{4,c1}$	0.0314	0.0431	295	492
$I_{3,c1}$	0.0173	0.00903	207	366

invariants. The number of fitting parameters is 4 in both cases. While the parameters for Fig. 4 were chosen in an *ad hoc* fashion, the invariants used in Fig. 3 are generated by a systematic procedure.

IV. $OH\cdot(H_2O)_7$

A. Unique configurations of cubic $OH\cdot(H_2O)_7$

Oriented graphs, which can be used to generate starting structures for quantum chemistry optimizations, for the $OH\cdot(H_2O)_7$ cubes were produced using automated graph theory techniques as described previously [13,24,48]. We also found that the same structures can be ascertained in another way: Each configuration of the cubic water octamer contains 16 hydrogens but only 12 hydrogen bonds; this leaves 4 dangling hydrogens on each cube. Therefore, there are a total of 56 dangling hydrogens among the 14 cubes which could be removed to generate $OH\cdot(H_2O)_7$ from $(H_2O)_8$, only 39 of which are symmetry-unique. Pictures of each structure are available in on-line supplementary materials [45]. For example, removal of any of the four dangling hydrogens from the $(H_2O)_8$ cubes of D_{2d}, S_4, or C_4 symmetry produces symmetry-equivalent $OH\cdot(H_2O)_7$ structures. This is illustrated for the D_{2d} isomer in Fig. 1. Each dangling hydrogen removed from $(H_2O)_8$ of C_1 symmetry generates a distinct $OH\cdot(H_2O)_7$ isomer. This is illustrated for the $C_{1(c)}$ isomer in Fig. 5.

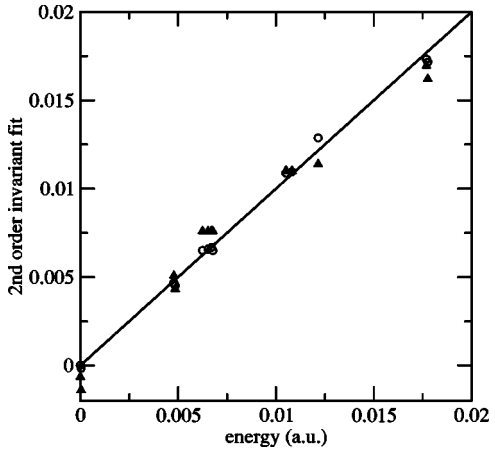

FIG. 4. Fit of the MP2 energies of the 14 octamers using topological properties *D*, *A*, and *B* from Ref. [14]. The filled triangles are fits using Belair and Francisco's topological properties *D*, *A*, and *B*. The open circles describe the fit using second order invariants.

The C_i and C_2 $(H_2O)_8$ structures each give rise to two distinct $OH\cdot(H_2O)_7$ isomers, while the C_s isomer generates three $OH\cdot(H_2O)_7$ isomers. In the following discussion, we will identify the $OH\cdot(H_2O)_7$ using a notation based on the $(H_2O)_8$ isomer from which they were generated by removal of a hydrogen. The $(H_2O)_8$ isomers are indicated by their names introduced in the previous section. We refer to the $OH\cdot(H_2O)_7$ structures with the symbols $P^{OH(R)}$ where *P* is the name of the parent structure and *R* is a number that distinguishes $OH\cdot(H_2O)_7$ structures generated from the same $(H_2O)_8$ isomer. The enumeration problem for $OH\cdot(H_2O)_7$ is equivalent to that for HF complexed with seven waters in a

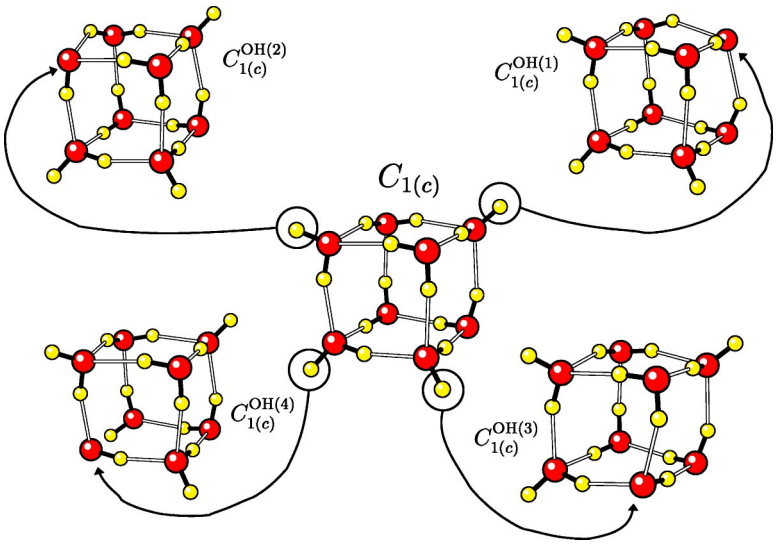

FIG. 5. The parent $(H_2O)_8$ isomer of C_1 symmetry (designated as $C_{1(c)}$ in our notation) is shown in the center of the figure. Removal of each of the 4 dangling hydrogens produces a distinct $OH\cdot(H_2O)_7$ isomer.

cubic structure, previously considered by Kuo and Klein, who found 39 symmetry-distinct structures of $HF(H_2O)_7$ [49].

Quantum chemistry optimizations were performed on all $OH\cdot(H_2O)_7$ structures as described above for the pure $(H_2O)_8$ clusters, and are tabulated in the on-line supplementary materials [45]. Each structure resulting from the initial PM3 optimization was equivalent in hydrogen bonding topology to its corresponding starting structure. The same was true for MP2 level optimizations that were started from the PM3 structures in all but two cases. Not surprisingly, these two cases were the two highest energy $(H_2O)_8$ isomers. The fate of these clusters upon optimization at the MP2 level is shown in Fig. 6. We were unable to locate local minima with these topologies. Instead, these two structures optimized to a different hydrogen bond topology than the other 37 optimized $OH\cdot(H_2O)_7$ structures, and therefore were not included in the graph invariant analysis.

The relative energies of the fully optimized $OH\cdot(H_2O)_7$ structures are plotted in Fig. 2 along with the relative energies of the corresponding $(H_2O)_8$ structures. The zero of energy for these two sets of data are taken to be the energies of D_{2d}^{OH} and D_{2d}, respectively. From this plotted data, it can be seen that, in general, the relative energies of the $OH\cdot(H_2O)_7$ structures follow fairly closely to the relative energies of their $(H_2O)_8$ parents (except for the two structures shown in Fig. 6). More precisely, the energy difference between a given radical structure and D_{2d}^{OH} is similar to the energy difference between the parent of that radical structure and D_{2d}. For example, the energy difference between D_{2d} and C_2 is 3.7 kcal/mol, whereas the difference between D_{2d}^{OH} and the two radical structures formed from C_2, namely, $C_2^{OH(1)}$ and $C_2^{OH(2)}$ are 4.0 and 3.2 kcal/mol, respectively. This trend is preserved for nearly all of the other structures. The stability of dimer arrangements within the $(H_2O)_8$ is reflected in the relative stability of the $OH\cdot(H_2O)_7$ clusters derived from the same $(H_2O)_8$ parent. When removal of a hydrogen from $(H_2O)_8$ disrupts a dimer, the resulting $OH\cdot(H_2O)_7$ cluster is less stable than when the hydrogen is removed from another part of the cluster. In Fig. 2 the energies of $OH\cdot(H_2O)_7$ clusters produced by disruption of a dimer unit are indicated with open squares. They are almost uniformly higher in energy than the other $OH\cdot(H_2O)_7$ clusters (filled squares).

These features strongly suggest that the structural properties responsible for the stability of the $OH\cdot(H_2O)_7$ structures are the same properties discussed in Sec. III that are responsible for the stabilities of the $(H_2O)_8$ parent structures. In terms of invariants, it suggests that there will be a high degree of transferability between the parameters for $(H_2O)_8$ and $OH\cdot(H_2O)_7$, an issue which is explored in the following section.

B. Simultaneous graph invariant analysis of $(H_2O)_8$ and $OH\cdot(H_2O)_7$

The 10 second order graph invariants needed to describe $(H_2O)_8$ and $OH\cdot(H_2O)_7$ are given in Eqs. (5)–(14). None of these 10 second order invariants are linearly dependent when evaluated over the 53 $(H_2O)_8$ and $OH\cdot(H_2O)_7$ isomers.

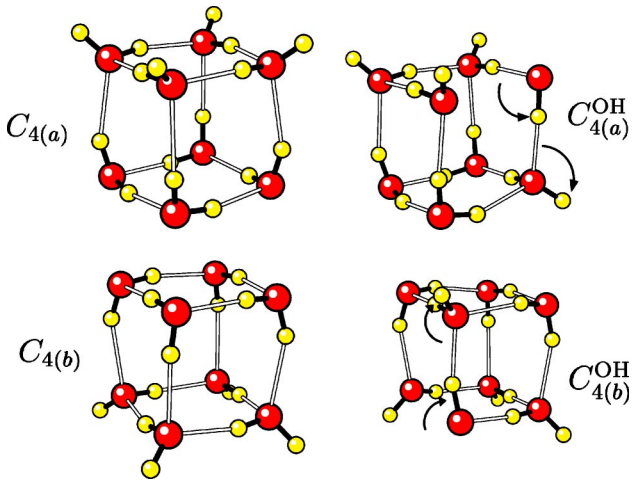

FIG. 6. The two highest energy $(H_2O)_8$ isomers, $C_{4(a)}$ and $C_{4(b)}$ (shown on the left), broke their starting H-bond topology upon optimization at the MP2 level. The displacement of hydrogen atoms in the $OH\cdot(H_2O)_7$ structures from the positions that would have maintained the topology is indicated with arrows on the right.

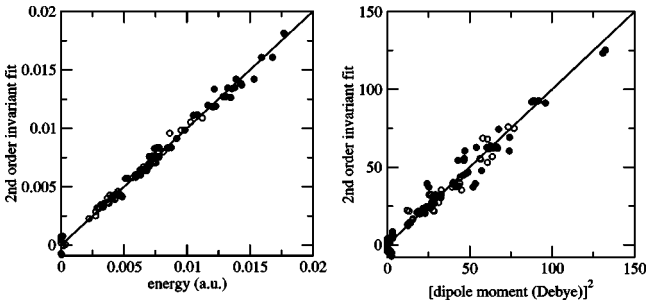

FIG. 7. Comparison of semiempirical PM3 (open circles) and *ab initio* MP2 results (filled circles) with fits to second order invariants for cubic $(H_2O)_8$ and $OH\cdot(H_2O)_7$. Energy is shown on the left and squared dipole moment on the right. The energy of the most stable $(H_2O)_8$ octamer is chosen as the zero of energy. The two isomers that are unstable as cubes at the MP2 level are excluded from those fits and are not shown in these plots. Those structures are included in the PM3 data.

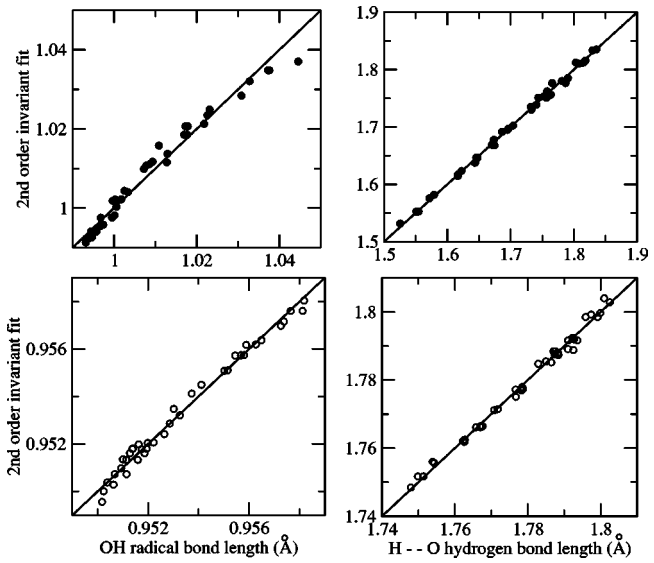

FIG. 8. Comparison of bond lengths associated with the OH radical with second order graph invariant fits. Filled circles are MP2 results while open circles are from PM3 calculations. The graphs in the left-hand column depict the bond length of the OH radical, while the graphs in the right-hand column show the distance from the hydrogen of the OH radical to the oxygen of the water molecule to which it is hydrogen bonded.

However, $I_{1,c1}$ evaluates to the zero vector because physically an OH from a water and hydroxyl radical do not occupy the same H-bond simultaneously. As a result, there are 9 independent second order invariant parameters available to describe the 53 $(H_2O)_8$ and $OH\cdot(H_2O)_7$ isomers. The quality of the second order invariant fit to all the cubic structures is depicted in Fig. 7.

The energy and squared dipole moment of both $(H_2O)_8$ and $OH\cdot(H_2O)_7$ are fit simultaneously in Fig. 7. The transferability of invariant parameters is confirmed by the comparison in Table II for the fitting coefficients for the 14 $(H_2O)_8$ isomers versus those for the 53 isomers for both $(H_2O)_8$ and $OH\cdot(H_2O)_7$.

We have emphasized that graph invariants are capable of describing how any scalar physical property depends on H-bond topology. An additional example of this capability is the dependence of bond lengths. In Fig. 8, two types of bond lengths associated with the OH radical are fit with second order invariants. First, the bond length of the radical itself is fit to the 8 second order invariants that are linearly independent over the 39 $OH\cdot(H_2O)_7$ isomers. In addition, the length of the H-bond connecting the OH radical to the oxygen of a water molecule is correlated with H-bond topology using invariants. The $OH\cdots O$ hydrogen bond length actually correlates best with the second order invariants. The OH radical bond length is not as well described by second order invariants, suggesting that it is controlled by many-body interactions and requires higher order invariants for a quantitative description.

V. CONCLUSIONS

Incorporation of a hydroxyl radical in an aqueous system opens new theoretical issues compared to pure water networks. OH binds more strongly to a water molecule as a hydrogen bond donor [6] than as a hydrogen bond acceptor [4]. Unlike the case of pure water, implicit in all the $OH\cdot(H_2O)_7$ structures we have calculated is the accommodation of a half-filled orbital whose orientation is determined by the local geometry surrounding the hydroxyl [6]. Despite the additional complexities of the situation, we find that the energetics and structure of $OH\cdot(H_2O)_7$ clusters is well captured by simple features of the local H-bond topology. This is reflected in the fact that the energy of $OH\cdot(H_2O)_7$ isomers relative to their $(H_2O)_8$ parent correlates with the number of dimer units (a double-acceptor donating to a double-donor) broken upon removal of a dangling hydrogen in the parent to form the $OH\cdot(H_2O)_7$ structure. These findings are consistent with recent work by Belair *et al.* on interactions between HO_2 and water [50]. They find that the H-bond topology immediately surrounding the radical species determines the radical-water binding mechanism.

As shown in Fig. 2, the correlation of $OH\cdot(H_2O)_7$ with dimer units broken is rather strong, but the trend is not perfect and there are clearly other factors at work. The graph invariant formalism [24] provides a route to a more quantitative relationship between local H-bond topology and physical properties. We have found that the lowest level graph invariants provide an excellent description of scalar physical properties of cubic $(H_2O)_8$ and $OH\cdot(H_2O)_7$. It is encouraging that there is a high degree of transferability between shared parameters for $(H_2O)_8$ and $OH\cdot(H_2O)_7$, indicating that topological features of the H-bond network may provide guidance in more complex and challenging situations, such as larger clusters, or the surface or interior of ice.

ACKNOWLEDGMENT

S.J.S. gratefully acknowledges the support of NSF Grant No. CHE-0109243.

[1] E. J. Lanzendorf, T. F. Hanisco, P. O. Wennberg, R. C. Cohen, R. M. Stimpfle, and J. G. Anderson, Geophys. Res. Lett. **28**, 967 (2001).
[2] T. Brauers, M. Hausmann, A. Bister, A. Kraus, and H.-P. Dorn, J. Geophys. Res., [Space Phys.] **106**, 7399 (2001).
[3] N. Carslaw *et al.*, J. Geophys. Res., [Space Phys.] **107**, 4190 (2002).
[4] K. S. Kim, H. S. Kim, J. H. Jang, H. S. Kim, B.-J. Mhin, Y. Xie, and H. F. Schaefer III, J. Chem. Phys. **94**, 2057 (1991).
[5] A. A. Nanayakkara, G. G. Balint-Kurti, and I. H. Williams, J. Phys. Chem. **96**, 3662 (1992).
[6] Y. Xie and H. F. Schaefer III, J. Chem. Phys. **98**, 8829 (1993).
[7] A. Engdahl, G. Karlström, and B. Nelander, J. Chem. Phys. **118**, 7797 (2003).
[8] P. D. Cooper, H. G. Kjaergaard, V. S. Langford, A. J. McKinley, T. I. Quickenden, and D. P. Schofield, J. Am. Chem. Soc. **125**, 6048 (2003).
[9] S. Hamad, S. Lago, and J. A. Mejías, J. Phys. Chem. **106**, 9104 (2002).
[10] P. Cabral do Couto, R. C. Guedes, B. J. Costa Cabral, and J. A. M. Simões, J. Chem. Phys. **119**, 7344 (2003).
[11] M. Roeselová, P. Jungwirth, D. J. Tobias, and R. B. Gerber, J. Phys. Chem. **107**, 12690 (2003).
[12] C. J. Gruenloh, J. R. Carney, C. A. Arrington, T. S. Zwier, S. Y. Fredericks, and K. D. Jordan, Science **276**, 1678 (1997).
[13] S. McDonald, L. Ojamäe, and S. J. Singer, J. Phys. Chem. A **102**, 2824 (1998).
[14] S. D. Belair and J. S. Francisco, Phys. Rev. A **67**, 063206 (2003).
[15] L. Pauling, J. Am. Chem. Soc. **57**, 2680 (1935).
[16] W. F. Giauque and J. W. Stout, J. Am. Chem. Soc. **58**, 1144 (1936).
[17] P. V. Hobbs, *Ice Physics* (Oxford, New York, 1974).
[18] V. F. Petrenko and R. W. Whitworth, *Physics of Ice* (Oxford, New York, 1999).
[19] E. A. DiMarzio and F. H. Stillinger, J. Chem. Phys. **40**, 1577 (1964).
[20] J. F. Nagle, J. Math. Phys. **7**, 1484 (1966).
[21] T. P. Radhakrishnan and W. C. Herndon, J. Phys. Chem. **95**, 10609 (1991).
[22] D. J. Anick, J. Mol. Struct.: THEOCHEM **587**, 87 (2002).
[23] D. J. Anick, J. Mol. Struct.: THEOCHEM **587**, 97 (2002).
[24] J.-L. Kuo, J. V. Coe, S. J. Singer, Y. B. Band, and L. Ojamäe, J. Chem. Phys. **114**, 2527 (2001).
[25] J.-L. Kuo and S. J. Singer, Phys. Rev. E **67**, 016114 (2003).
[26] J.-L. Kuo, C. V. Ciobanu, L. Ojamäe, I. Shavitt, and S. J. Singer, J. Chem. Phys. **118**, 3583 (2003).
[27] D. J. Anick, J. Phys. Chem. **107**, 1348 (2003).
[28] D. J. Anick, J. Chem. Phys. **119**, 12442 (2003).
[29] R. Whitworth, Can. J. Phys. **81**, 123 (2003).
[30] R. Podeszwa and V. Buch, Phys. Rev. Lett. **83**, 4570 (1999).
[31] C. Kobayashi, S. Saito, and I. Ohmine, J. Chem. Phys. **113**, 9090 (2000).
[32] C. Kobayashi, S. Saito, and I. Ohmine, J. Chem. Phys. **114**, 1440 (2000).
[33] C. Kobayashi, S. Saito, and I. Ohmine, J. Chem. Phys. **115**, 4742 (2000).
[34] J. P. Cowin, A. A. Tsekouras, M. J. Iedema, K. Wu, and G. B. Ellison, Nature (London) **398**, 405 (1999).
[35] S. J. Singer, J.-L. Kuo, T. K. Hirsch, C. Knight, L. P. Ojamäe, and M. L. Klein (unpublished).
[36] L. Ojamäe, I. Shavitt, and S. J. Singer, Int. J. Quantum Chem., Quantum Chem. Symp. **29**, 657 (1995).
[37] L. Ojamäe, I. Shavitt, and S. J. Singer, J. Chem. Phys. **109**, 5547 (1998).
[38] C. J. Tsai and K. D. Jordan, J. Phys. Chem. **97**, 5208 (1993).
[39] C. Møller and M. Plesset, Phys. Rev. **46**, 618 (1934).
[40] R. J. Bartlett and D. M. Silver, Int. J. Quantum Chem., Symp. **8**, 271 (1974).
[41] J. S. Binkley and J. A. Pople, Int. J. Quantum Chem. **9**, 229 (1975).
[42] R. J. Bartlett and D. M. Silver, Int. J. Quantum Chem., Symp. **9**, 183 (1975).
[43] J. A. Pople, J. S. Binkley, , and R. Seeger, Int. J. Quantum Chem., Symp. **10**, 1 (1976).
[44] M. J. Frisch *et al.*, *Gaussian 98* (Gaussian, Inc., Pittsburgh, PA, 2002), revision A.11.3.
[45] See EPAPS Document No. E-PLRAAN-71-028501 for tabulated energies and pictures of each of the cubic $(H_2O)_8$ and $OH\cdot(H_2O)_7$ structures. A direct link to this document may be found in the online article's HTML reference section. The document may also be reached via the EPAPS homepage (http://www.aip.org/pubservs/epaps.html) or from ftp.aip.org in the directory /epaps/. See the EPAPS homepage for more information.
[46] J. D. Bernal and R. H. Fowler, J. Chem. Phys. **1**, 515 (1933).
[47] J. J. P. Stewart, J. Comput. Chem. **10**, 209 (1989); **10**, 221 (1989).
[48] M. D. Tissandier, S. J. Singer, and J. V. Coe, J. Phys. Chem. A **104**, 752 (2000).
[49] J.-L. Kuo and M. L. Klein, J. Chem. Phys. **120**, 4690 (2004).
[50] S. D. Belair, H. Hernandez, and J. S. Francisco, J. Am. Chem. Soc. **126**, 3024 (2004).